crystals

MDPI

Review

Floating Zone Growth of Pure and Pb-Doped Bi-2201 Crystals

Maria Roslova, Bernd Büchner and Andrey Maljuk *

Leibniz Institute for Solid State and Materials Research Dresden (IFW Dresden), 01069 Dresden, Germany; m.roslova@ifw-dresden.de (M.R.); b.buechner@ifw-dresden.de (B.B.)
* Correspondence: a.malyuk@ifw-dresden.de

Abstract: In this review, we summarize recent progress in crystal growth and understanding of the influence of crystal structure on superconductivity in pure and Pb-doped $Bi_2Sr_2CuO_y$ (Bi-2201) materials belonging to the overdoped region of high-temperature cuprate superconductors. The crystal growth of Bi-2201 superconductors faces challenges due to intricate materials chemistry and the lack of knowledge of corresponding phase diagrams. Historically, a crucible-free floating zone method emerged as the most promising growth approach for these materials, resulting in high-quality single crystals. This review outlines the described methods in the literature and the authors' synthesis endeavors encompassing Pb-doped Bi-2201 crystals, provides a detailed structural characterization of as-grown and post-growth annealed samples, and highlights optimal growth conditions that yield large-size, single-phase, and compositionally homogeneous Bi-2201 single crystals.

Keywords: Bi-2201; floating zone crystal growth; crystal structure; cuprates; superconductivity

1. Introduction

It is commonly believed that superconductivity is more conventional in overdoped cuprates [1–3]. Transport and spectroscopic studies suggest that the non-superconducting ground state is more 'normal', and the superconducting (SC) state exhibits Bardeen–Cooper–Schrieffer (BCS) *d*-wave features [4]. However, recent experiments have shown unconventional behavior in strongly overdoped cuprates in both normal [5,6] and superconducting states [7,8]. The $Bi_2Sr_2CuO_y$ (Bi-2201) cuprate came into focus due to recent investigations unraveling its unique features: the presence of a pseudogap in the overdoped side of the electronic phase diagram, which questions the scenario of the pseudogap phase crossing the superconducting dome [9], and a Lifshitz transition from a hole-like Fermi surface topology to an electron-like Fermi surface topology occurring at the doping level where the sample becomes non-superconducting [10]. In addition, circular and linear photogalvanic measurements transition revealed that the pseudogap regime in both Bi-2201 [11] and Bi-2212 ($Bi_2Sr_2CaCu_2O_y$) [12] families marks a phase transition associated with the development of chiral and inversion symmetry breaking. Reducing the symmetry of a superconducting material modifies the properties of the superconducting states, e.g., recently, a spin texture with nonzero spin polarization was found in Bi-2212 [13], which could be caused either by an absence of any inversion center in the structure or local symmetry breaking due to structural distortions typical for cuprates. Several other investigations of the closely related doped Bi-2212 system also raise doubts regarding the centrosymmetry of the crystal structure [12,13].

The superconducting Bi-2201 has a relatively simple crystallographic structure, possessing only one copper oxide block in the unit cell, as well as a simple electronic band structure, providing an excellent platform for comparing density functional theory calculations with direct band structure probes. In contrast, two-layered $Bi_2Sr_2CaCu_2O_y$ and three-layered $Bi_2Sr_2Ca_2Cu_3O_y$ materials have significant band structure splitting [14], which complicates the interpretation of angle-resolved photoemission spectroscopy (ARPES) and scanning tunneling microscopy (STM) results.

Citation: Roslova, M.; Büchner, B.; Maljuk, A. Floating Zone Growth of Pure and Pb-Doped Bi-2201 Crystals. *Crystals* **2024**, *14*, 270. https://doi.org/10.3390/cryst14030270

Academic Editor: Evgeniy N. Mokhov

Received: 12 February 2024
Revised: 28 February 2024
Accepted: 5 March 2024
Published: 11 March 2024

From a physical standpoint, it seems rational to examine the relationships between superconductivity and the pseudogaps in low T_c cuprates. As it is simplified, a proper disentanglement of superconducting and pseudogap features because thermal fluctuations become much less pronounced once the temperature approaches 0 K. Therefore, a pure $Bi_2Sr_2CuO_y$ compound was suggested to be a promising model system. And in turn, angular-dependent magnetoresistance [15] and intrinsic tunneling [16] studies in Bi-2201 cuprate with T_c~3–4 K revealed the large disparity between superconducting and pseudogap scales.

It is known that by partially substituting Bi with Pb in Bi-2201, together with annealing under different conditions, the samples can be pushed to the overdoped and heavily overdoped regions to even become non-superconducting. However, doping does not change the value of T_c in a systematic way; rather, it strongly depends on synthesis conditions, and different synthesis protocols may result in samples with different T_c. Apparently, floating zone crystal growth results in high-quality single crystals of undoped and Pb-doped Bi-2201 with a homogenous composition distribution along the crystal ingot [17,18], but it is quite time-consuming. Therefore, there is a very limited number of reports on crystal growth using this technique, and only a few structural works on such crystals have been available in the literature since the 80s. In this review, we focus particularly on the floating zone growth of Pb-doped Bi-2201 crystals and compare crystal structures of two heavily doped as-grown and post-growth annealed samples with corresponding T_c = 3 K and 23 K.

2. State of the Art

2.1. Crystal Growth

The first pure Bi-2201 samples were prepared using the flux technique, using either self-flux (CuO-based flux) [19] or KCl-flux [20]. Unfortunately, as recognized later, flux-prepared samples always suffer from several drawbacks [21]: (1) crucible material contamination due to melt corrosion at high temperatures; (2) flux impurities in as-grown samples; (3) small samples (<2 mm) in the (a,b)-plane while the typical thickness along the c-axis is less than 0.1 mm; (4) mechanical detaching of crystals from a solidified melt often causes sample damage; (5) small yield growth. Moreover, possible K and Cl pollution has to be considered for KCl-flux-grown samples. Another dramatic problem is that flux-prepared crystals show scant reproducibility of superconductivity [21]. For example, Bi-2201 samples were fabricated by the CuO self-flux technique in $Zr(Y)O_2$ (YSZ), Al_2O_3, and Au containers in Sonder et al. [22]. The superconductivity in samples grown in alumina containers was not well reproducible. A number of crystals demonstrated a broad SC transition using resistivity measurements, but none of them showed a well-defined SC transition using magnetization measurements. On the other hand, the superconductivity onset in Bi-2201 samples fabricated in either YSZ or Au containers was well reproducible. Both resistivity and magnetization measurements proved the presence of bulk superconductivity, although the width of the superconducting transition was unusually broad [22]. The authors carried out high-precision chemical analysis of the sample content using spark-source mass spectroscopy. Obviously, Al was detected in Bi-2201 samples prepared in the Al_2O_3 container but at very low levels of 10–50 ppm. Concurrently, samples grown in YSZ crucibles had remarkably higher concentrations of both Zr (20–70 ppm) and Y (50–120 ppm). All crystals fabricated in Au containers had no visible sign of Au pollution (Au content < 5 ppm), according to this chemical analysis. The Al pollution response to superconductivity in Bi-2201 crystals has not yet been well understood. Besides these drawbacks, all flux-prepared crystals have been rather small, typically $4 \times 4 \times 0.02$ mm^3 in size [22]. Thermogravimetric measurements revealed oxygen deficiency in pure as-grown Bi-2201 crystals, varying from about 0.1 to 0.5 oxygen per formula unit. This effect depends on a sample's proximity to a melt surface. Annealing in oxygen flow changes the resistivity behavior from semiconducting (as-grown crystal) to metallic (oxygen annealed) [22].

The crucible-free floating zone (FZ) method allows one to overcome nearly all of the abovementioned drawbacks of the flux technique. This method was successfully used for

the crystal preparation of many other high-T_c cuprates, including Sr-doped La_2CuO_4 [23] and Bi-2212 [24]. However, the first $Bi_2Sr_2CuO_y$ samples grown by the FZ technique did not demonstrate any superconductivity and were often flake-like [25]. All attempts to improve superconducting properties by post-growth heat treatment in oxygen/argon flow failed. The first superconducting [18] and bulk $Bi_2Sr_2CuO_y$ samples applicable even to inelastic neutron measurements [21] were prepared only in the late 90s. Nevertheless, it was noted that T_c varied from sample to sample, and some crystals collected from the same ingot failed to show any superconductivity, although other samples were superconducting. The authors [21] could not find a difference between these crystals either in composition (by EDX) or in their powder XRD patterns. A similar effect was observed on FZ-grown $PrBa_2Cu_3O_{7-y}$ samples [26]. From a growth point of view, the FZ fabrication of undoped and Pb-doped Bi-2201 samples seems very similar. Consequently, we will mostly discuss the intricate details of FZ growth for lead-doped samples. Also, we do not investigate either the CuO-flux [27] or FZ growth of La-doped Bi-2201 crystals due to the composition inhomogeneity problems in as-grown ingots [28].

2.2. Crystal Structure

In terms of crystal structure, Bi-based cuprates are intergrowths of two BiO sheets with n (n = 1, 2, 3. . .) copper oxide perovskite-like layers [17]. The first member (n = 1) is named after its nominal stoichiometric composition, Bi-2201. Although early structural studies on superconducting Bi-2201 from powder XRD data have suggested a tetragonal structure with the space group $I4/mmm$ and lattice parameters a_t = 3.8097(4) Å and c_t = 24.607(3) Å [29], subsequent single crystal X-ray diffraction (SCXRD) and electron diffraction studies revealed that it possesses an orthorhombic structure with inequivalent a and b axes, which may be accompanied by minor monoclinic distortion (Mironov et al. [30]). While in-plane lattice anisotropy is absent in Bi-2212 (n = 2) and CCOC ($Ca_{2-x}Na_xCuO_2Cl_2$) compounds, it was found to be important for, e.g., YBCO and $La_{2-x}Sr_xCuO_4$ materials [31]. The space group *Cccm* has typically been suggested for the parent Bi-2201 in the literature (Torardi et al. [32], Leligny et al. [33]), with lattice parameters of approx. $a_t\sqrt{2}\times c_t \times a_t\sqrt{2}$ and often the space group denoted as *Amaa* or *Bbmb*. In non-conventional settings, the orthorhombic long axis is set to be co-directional with the pseudo-tetragonal one. Ito et al. [34] reported the first SCXRD crystal structure solved from a heavily Pb-doped Bi-2201 crystal grown by the floating zone growth technique. At a Pb/(Bi + Pb) ratio of 0.15, it was found to possess the space group *Cccm* with the lattice parameters a = 5.392(3) Å, b = 24.603(5) Å, c = 5.300(3) Å, and V = 703.2(5) Å^3 [34].

Although most authors consider *Amaa* or its subgroup $A2/a$ for the structure description of undoped Bi-2201 (see Torardi et al. [32], Leligny et al. [33], Mironov et al. [30]), it is worth noting that several cases of closely related non-centrosymmetric structures have also been known, e.g., Tarascon et al. [35] reported structures of modulation-free non-superconducting $BiPbSr_2MO_y$ phases (M = Co, Mn, Fe) possessing the space group $A2aa$, and Gao et al. [36] proved the space group $A2aa$ for an average structure of a Pb-doped single layer $Bi_2Sr_{2-x}Ca_xCuO_6$ cuprate and the Aa symmetry of a satellite diffraction pattern.

An average crystal structure of Bi-2201 possesses single sheets of corner-sharing CuO_4 units in which each copper atom has two additional oxygen atoms positioned above and below the sheet to form an axially elongated (Jahn–Teller-distorted) octahedron. These Cu-O planes are separated by Bi-O and Sr-O layers formed by distorted MO_6 edge-shared octahedra. Cu-O layers in the superconducting orthorhombic Bi-2201 phase may be buckled. It is known that local lattice distortions produced by chemical inhomogeneity can reduce the value of T_c in a systematic way: the larger the Cu-O plane buckling angle, the lower the T_c. Nevertheless, the T_c of superconducting Bi-2201 species varies, and these variations are sensitive to multiple internal structural features. Buckling alone is not sufficient to characterize properties associated with superconductivity—thus, the stoichiometric monoclinic Bi-2201 phase was found to contain periodic crystallographic shears interrupting the connections of the flat CuO_2 planes [37], leading to insulating

behavior [38]. In contrast, superconducting Tl-2201 (T_c around 90 K) has a tetragonal structure with nearly perfectly flat Cu-O layers and a slight buckling in the Tl-O and Ba-O layers [32].

In the literature, two distinct "2201" phases with closely related compositions are described: the off-stoichiometric orthorhombic phase, exhibiting superconductivity (also called the Raveau phase), and a stoichiometric monoclinic $Bi_2Sr_2CuO_6$ phase. It is worth noting that the composition of the orthorhombic Raveau phase is always off-stoichiometric with the partial substitution of Bi for Sr since it forms a $Bi_{2+x}Sr_{2-x}CuO_y$ solid solution with 0.1 5 $\leq x \leq$ 0.4 [39]. The perfectly stoichiometric Bi-2201 compound is an insulator and has a monoclinic unit cell with a = 24.451(5) Å, b = 5.425(2) Å, c = 21.954(5) Å, and β = 105.41(1)^0 [37] and is sometimes named a "collapsed" Bi-2201 since its c_t axis is 1 Å shorter than those of superconducting Bi-2201. The structure is derived from that of the pseudo-tetragonal 2201 phase by a periodic crystallographic shear parallel to the c_t axis. Periodic slabs of 2201 with a thickness of eight octahedra are then formed [37], as shown by HRTEM observations.

A well-known structural feature in the Bi-based high-T_c superconductors is an incommensurate modulation, appearing due to metal atoms as well as oxygen disorder in Bi-O and Sr-O layers or (CuO_2) planes, caused by a mismatch in the perovskite and rock salt blocks of the structure. Despite the close resemblance in average structures between the 2201 and 2212 ($Bi_2Sr_{2-x}Ca_xCuO_6$) systems, a distinct difference exists in the modulation type in these structures. While modulation in the 2212 phase has a wave vector of 0.21a*, modulation in the 2201 phase has been described by two wave vectors with q_1 = 0.21a* + 1/3c* and q_2 =0.21a* − 1/3c* (sp.gr. *Amaa* was used in the original works). An influence of Pb substitution on the satellite pattern is also evident: doping of the 2201 phase leads to a disappearance of the satellites in an X-ray pattern, while Pb doping of the Sr/Ca 2212 phase gives a diffraction pattern with two different q vectors, both in the a* direction [40]. Another approach was suggested by considering the Bi-containing mixed oxide structures as composites [41], with the oxygen in the Bi-O layer forming the second sublattice, while all other atoms belong to the first one. Refinement of the composite structure was taken by Yamamoto et al. [42], and a correlation was revealed between the q-vector and the extra oxygen content within the Bi-O layer.

3. Results

3.1. Floating Zone Crystal Growth of Pb-Doped Bi-2201 at IFW Dresden

The large-size lead-doped Bi-2201 crystals were fabricated for the first time in 1997 by the crucible-free FZ method [18]. Prior to growth, an as-sintered feed rod was pre-melted at a fast rate of 25–27 mm/h in an infrared (IR) image furnace in order to obtain a high-density rod with a density above 90% of the crystal density. For the feed rod preparation, Bi_2O_3, PbO, $SrCO_3$, and CuO powders of at least 3N purity were used as starting materials. A number of feed rod compositions were investigated. The initial powder mixture was mixed in ethanol and fired at 720–840 °C for 1 day in air. The rods were pressed at 1 kbars by a cold isostatic press and finally fired at 840 °C for 1 day in air. The best feed rod composition was detected to be $Bi_{1.74}Pb_{0.38}Sr_{1.88}CuO_y$. Crystal growth was initiated by forming a molten zone between the feed and seed rods using IR heating, and the zone was passed through the feed rod at a rate of 5.0 to 0.3 mm/h [18].

Large-size and bulk $Bi_{1.6}Pb_{0.4}Sr_{2.05}CuO_y$ single crystals were grown at IFW Dresden in a similar way. A four-mirror-type image furnace produced by CSI (Japan) equipped with 4 × 300 W halogen lamps was used for the growth, see Figure 1. We found that using the pre-melted feed rod does play an important role in a stable growth run because liquid penetration onto a feed rod was strongly suppressed in this case [21]. Therefore, for a high-density pre-melted feed rod, a stable molten zone (MZ) could be maintained over a long-lasting experiment (over 1–2 days). In contrast, using low-density as-sintered rods with a density of less than 75% always terminated FZ growth due to dramatic liquid penetration. Thus, a straight, high-density, and equal-diameter pre-melted rod was crucial to stabilizing

MZ for long-lasting growth. Also, similar to undoped Bi-2201, a high temperature gradient (~150–300 °C/cm) in a hot zone generated by correctly focused halogen lamps was needed to maintain a stable molten zone. A long (about 10 mm in length) pre-melted rod was cut into two pieces, and the shorter piece (~2 cm in length) was utilized as a seed and the longer one as a feed rod. Both feed and seed rods were coaxially mounted on upper and lower shafts inside a transparent quartz tube. The used O-ring sealing was gas-tight and protected the growth atmosphere from air humidity. Slow growth rates of 0.5–1.0 mm/h were applied in order to achieve faster grain selection. Both feed and seed rods were counter-rotated (15–20 rpm) to provide homogeneous temperature distribution in a radial direction. The bulk Pb-substituted Bi-2201 crystals with an actual composition of $Bi_{1.8}Pb_{0.38}Sr_{2.01}CuO_y$ were successfully fabricated using the CSI image furnace with infrared heating. Growth was performed in an $Ar/O_2 = 90/10$ gas mixture, and the actual pulling rate was 1.0–0.8 mm/h. As-grown samples were non-superconducting above 4 K from the magnetization measurements and demonstrated a superconducting transition at T_c~22–23 K after post-growth heat treatment under vacuum conditions [18].

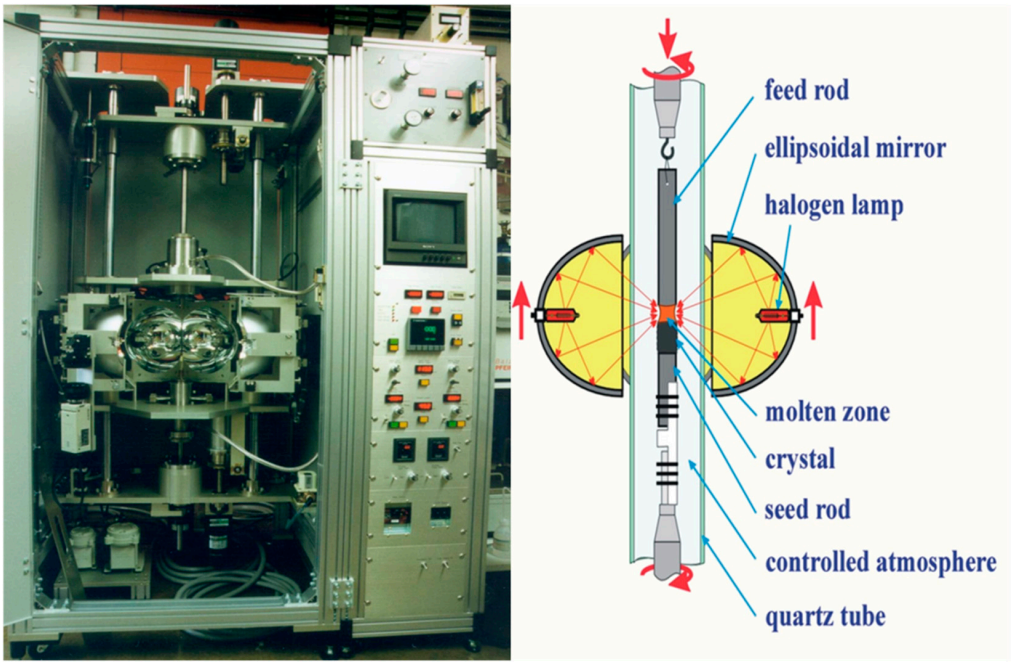

Figure 1. A photo of the image furnace with optical heating installed at IFW Dresden (produced by CSI, Japan). Reproduced from Ref. [17], with permission from Springer International Publishing, copyright 2016.

The Pb-doped Bi-2201 single crystals cleaved by a sharp scalpel from as-grown ingot are depicted in Figure 2 (left). The biggest samples had dimensions of up to $15 \times 4 \times 3$ mm^3 with a clear (010) cleavage plane. The weak PbO and Bi_2O_3 evaporation from MZ was detected during growth. The boiling points of PbO and Bi_2O_3 oxides were 1480 °C and 1890 °C, respectively. The evaporated material deposits on the inner wall of the quartz tube formed a slightly yellowish thin layer. Therefore, IR heating was not affected by it. Therefore, there was no need to increase the lamp's power, and in turn, MZ remained stable over the growth.

Typically, $Bi_{1.6}Pb_{0.4}Sr_{2.05}CuO_y$ samples with thicknesses of up to 3 mm along the c-axis showed a broadening of neutron rocking curves due to weak shoulders around a few Bragg peaks, reflecting the co-existence of slightly misoriented grains. The mosaicity of these crystals was found to be around 2–3°. In contrast, crystals with a thickness of 0.3–0.5 mm along the c-axis demonstrated better mosaicity of about 0.5–0.7° [17].

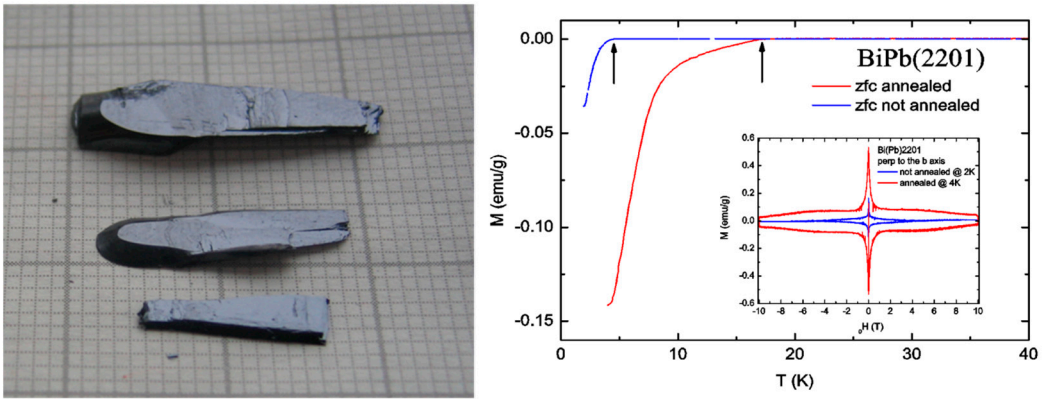

Figure 2. (**Left**) The Bi(Pb)-2201 samples cleaved from as-grown ingot. (**Right**) Superconducting transitions in as-grown and argon-annealed lead-doped Bi-2201 crystals. Arrows indicate T_c onset. Reproduced from Ref. [17] with permission from Springer International Publishing, copyright 2016.

As-grown lead-substituted Bi-2201 crystals are usually non-superconducting above 3 K, but post-growth heat treatment in a vacuum (10^{-5} mbar) dramatically enhances T_c up to 22–23 K (Figure 2, right). Annealing conditions and the effects of heat treatment on the superconductivity and material stability of $Bi_{1.6}Pb_{0.4}Sr_{2.05}CuO_y$ crystals are summarized in Table 1 [17]. Since the substitution of Bi^{3+} with Pb^{2+} is believed to generate holes in a crystal lattice, doping by lead makes the Bi-2201 compound "heavily overdoped".

Table 1. Annealing conditions, phase stability, and superconductivity of $Bi_{1.6}Pb_{0.4}Sr_{2.05}CuO_y$ samples. Adapted from Ref. [17].

Sample Composition	Annealing Temperature	Annealing Time/Atmosphere	Superconducting Temperature [1]	Stability in Air
$Bi_{1.6}Pb_{0.4}Sr_{2.05}CuO_y$	As-grown	-	3 K	Yes
$Bi_{1.6}Pb_{0.4}Sr_{2.05}CuO_y$	723 K	7 days/O_2	Non-superconducting	Yes
$Bi_{1.6}Pb_{0.4}Sr_{2.05}CuO_y$	723 K	10 days/Ar	13 K	Yes
$Bi_{1.6}Pb_{0.4}Sr_{2.05}CuO_y$	723 K	7 days/vacuum	17 K	Yes
$Bi_{1.6}Pb_{0.4}Sr_{2.05}CuO_y$	823 K	5 days/vacuum	23 K	No
$Bi_{1.6}Pb_{0.4}Sr_{2.05}CuO_y$	923 K	3 days/vacuum	No measurement	Decomposed

[1] T_c was determined from magnetization measurements.

Low-temperature superconductivity does vanish in as-grown samples after annealing in oxygen flow (at least, T_c is below the low-temperature limit of 2 K at our experimental facility). In contrast, annealing of as-grown lead-doped Bi-2201 samples in a vacuum (~10^{-5} mbar) at 823 K for 5 days increases T_c up to 22–23 K. This is a direct hint that extra oxygen expels from as-grown Pb-doped Bi-2201 samples, reflecting a reduction in sample doping from heavily to slightly overdoped. By adjusting the annealing atmosphere and temperature, the superconductivity transition temperature could be varied between 0 and 23 K. Nevertheless, the lead-substituted Bi-2201 samples became air sensitive after post-growth heat treatment under vacuum conditions above 823 K. These crystals were completely powdered after keeping on a desk at room temperature for a week. Only crystals annealed either in Ar flow (5N purity) or in a vacuum below 723 K remained stable in air, had no visible signs of crystal decomposition and retained superconductivity. Thus, superconductivity in lead-doped Bi-2201 material is highly sensitive to the annealing process and may result in samples with various T_c if the heat treatment is carried out under different conditions [43]. It has been found in the literature that the whole region from slightly overdoped to heavily overdoped samples can be covered by combining Pb^{2+} partial doping with annealing in a reduced atmosphere.

Concerning the effect of lead doping on structural modulation, it was found that modulation is preserved by La doping, while the substitution of Pb for Bi acts effectively in modulation suppression [44]. It was shown by Ikeda et al. [45] that structural modulation was no longer present at a lead-solubility of $x = 0.4$ at $y = 0.125$ in $Bi_{2-x}Pb_xSr_{2-y}CuO_z$.

3.2. SCXRD Investigations on Pb-Doped Bi-2201

The majority of previous structural characterization works for the Bi-2201 family of cuprates were performed on crystals grown from off-stoichiometric oxide mixtures. Therefore, the "best" crystals chosen for SCXRD might not always be representative of the bulk. Floating zone crystal growth, in contrast, guarantees a homogenous composition distribution along a crystal ingot [17,18], which is beneficial for the reproducibility of SCXRD analysis, too. Unfortunately, there are only a few reports about crystal growth by this technique, and consequently, only a few structural works on such crystals have been available since the 80s [34]. In this section, we thoroughly analyzed centrosymmetry as well as modulation suppression on two heavily Pb-doped Bi-2201 crystals before and after post-growth annealing.

Single crystal X-ray diffraction data acquisition was accomplished on a Bruker D8 Venture (MoKα λ = 0.71073 Å) equipped with a PHOTON 100 CMOS detector. The measurements were performed at room temperature. Indexing was performed using APEX3 software [46]. Data integration and absorption corrections were performed using the SAINT and SADABS software [46,47], respectively. Crystal structure was solved by dual-space methods implemented in the SHELXT [48] program and refined by the full-matrix least-squares method on F^2 with SHELXL [49]. The composition of the crystal was taken from EDX analysis.

Generally, our SCXRD data confirmed the average crystal structure of Pb-doped Bi-2201 described in the literature. SCXRD reflections can indeed be indexed in a *C*-centered orthorhombic cell with very close values of lattice parameters a = 5.388(2) Å, b = 24.608(1) Å, and c = 5.279(2) Å (a non-annealed crystal with T_c = 3 K, further denoted as OD3K), or a = 5.3947(6) Å, b = 24.605(3) Å, and c = 5.2786(6) Å (an annealed crystal with T_c = 23 K, further denoted as OD23K). A notable feature of the OD23K crystal is a very weak incommensurate modulation with $q \approx 0.21\ c^*$, clearly seen in the 0*kl* reciprocal layers (see Figure 3). For comparison, the OD3K crystal demonstrates rather thin diffuse streaks along a^* instead of well-defined spots of satellite reflections, see Figure 4. This modulation in OD23K cannot be entirely associated with post-annealing, as it is also present in the sample before annealing. The mismatch between the BiO-slab and the copper oxide perovskite block cannot be eliminated by Pb doping alone, and the observed modulation is evidently a residual feature. The q-vector value is close to those reported by Gao et al. [36] for a Pb-doped single layer $Bi_2Sr_{2-x}Ca_xCuO_6$ cuprate as well as to those previously reported for undoped Bi-2212 [50] ($q \approx 0.21\ a^*$, sp.gr. *Amaa* was used in the original works). In contrast, some literature reports a full disappearance of the satellite patterns in heavily Pb-doped Bi-2201 [34,45]. In the following discussion, we show that these weak reflections can be convincingly described in the non-centrosymmetric space group *Ccc*2.

The Pb,Bi-2201 structure can be solved and refined either in the centrosymmetric *Cccm* or in the non-centrosymmetric *Ccc*2 space group. It is worth noting that E-statistics indicate that the structure is rather non-centrosymmetric, as Sheldrick's $|E^2 - 1|$ criterion is 0.769; see Figure 5, data for the OD23K crystal.

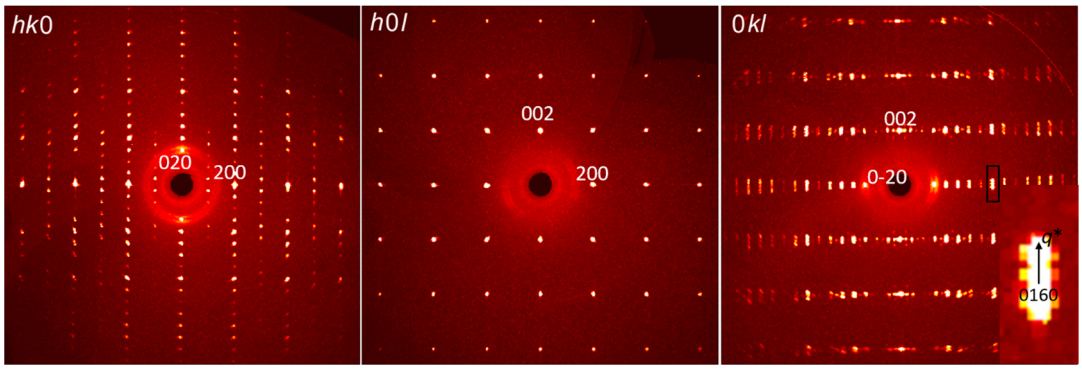

Figure 3. Recalculated reciprocal layers *hk*0, *h*0*l*, and 0*kl* for an annealed OD23K crystal with T_c = 23 K, and composition Pb:Bi:Sr:Cu = 0.35(3):1.69(8):2.01(9):1, Pb/(Bi + Pb) ratio is 0.17. A disappearingly weak incommensurate modulation with $q \approx 0.21$ c^* preserves even at very high Pb concentrations in Pb,Bi-2201; see the inset.

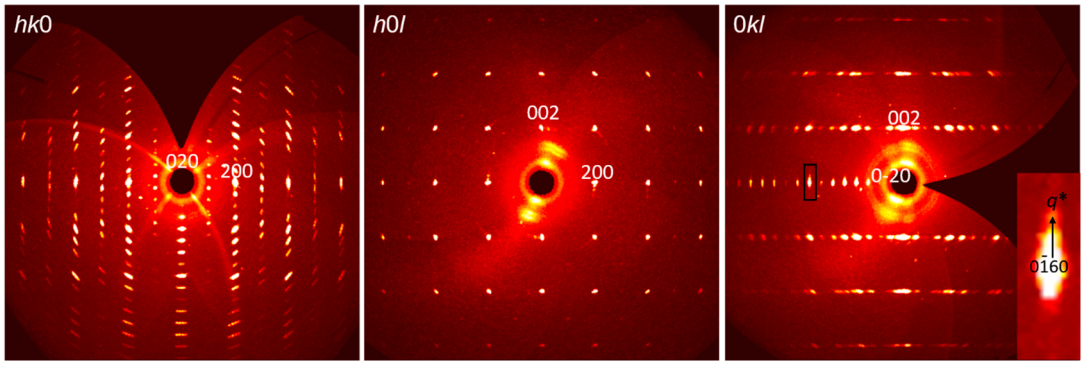

Figure 4. Recalculated reciprocal layers *hk*0, *h*0*l*, and 0*kl* for a non-annealed OD3K crystal with T_c = 3 K, and composition $Bi_{1.6}Pb_{0.4}Sr_{2.05}CuO_y$ Pb:Bi:Sr:Cu = 0.4:1.6:2.05:1, Pb/(Bi + Pb) ratio is 0.2.

We tested both *Cccm* and *Ccc*2 solutions and ascertained that the positions of the metal atoms Bi, Sr, and Cu found using an ab initio structure solution by SHELXT are basically equivalent in both space groups. However, refined anisotropic temperature factors (ADP) for the metal atoms, as well as crystallographic coordination of the Bi/Pb by O atoms, are clearly different. The structure solution in space group *Cccm* showed a structural arrangement very similar to one described previously for the parent 2201 phase, with ribbons of strong Bi-O bonds and splitting of the oxygen site in the Bi-plane. Moreover, the Bi atoms in this model had very large anisotropic factors along the *c*-axis.

Lowering symmetry to *Ccc*2 and the refinement of this model resulted in R_1 = 4.78% and reasonable ADP along the *c*-axis. The atomic coordinates, temperature factors, and site occupancies for the Bi-2201 crystal, together with the details of the refinement, are listed in Tables S1–S3. As can be seen from these tables, the stereochemistry of the various ions is as expected for this structure type (Figure 6). Distinct from Y. Ito et al. [51], where the Pb dopant was placed in both Bi and Sr sites, we assume that the Sr sites are occupied predominantly by Sr, whereas Pb/Bi sites are mixed occupied. Since the scattering powers of Pb and Bi are almost equal for wavelengths that are not close to an absorption edge, these atoms cannot be distinguished by conventional X-rays. The experimental composition measured by EDX and averaged over all measurements was found to be Pb:Bi:Sr:Cu = 0.35(3):1.69(8):2.01(9):1, and the Pb/(Bi + Pb) ratio was 0.17; thus, the Cu oxidation state can be estimated as +2.21, providing an ideal oxygen composition. SCXRD refinement revealed that the Pb/Bi site might be slightly underoccupied compared with the EDX data. There is no extra oxygen position found within the Bi-O layers, in contrast to the undoped Bi-2201, e.g., Mironov et al. [30].

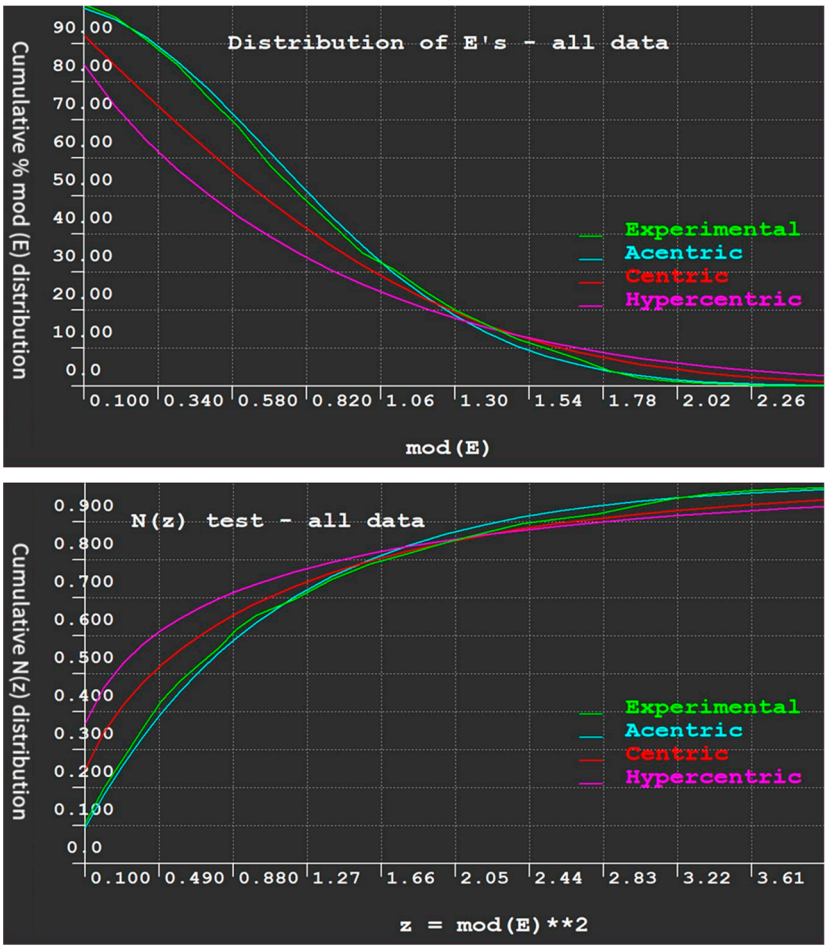

Figure 5. E-statistics indicate the structure of Pb-doped Bi-2201 is non-centrosymmetric. The probability that the structure is centrosymmetric is only 18.5%. Sheldrick's $|E^2 - 1|$ criterion is 0.769 (ideal values CENTRIC = 0.968, ACENTRIC = 0.736).

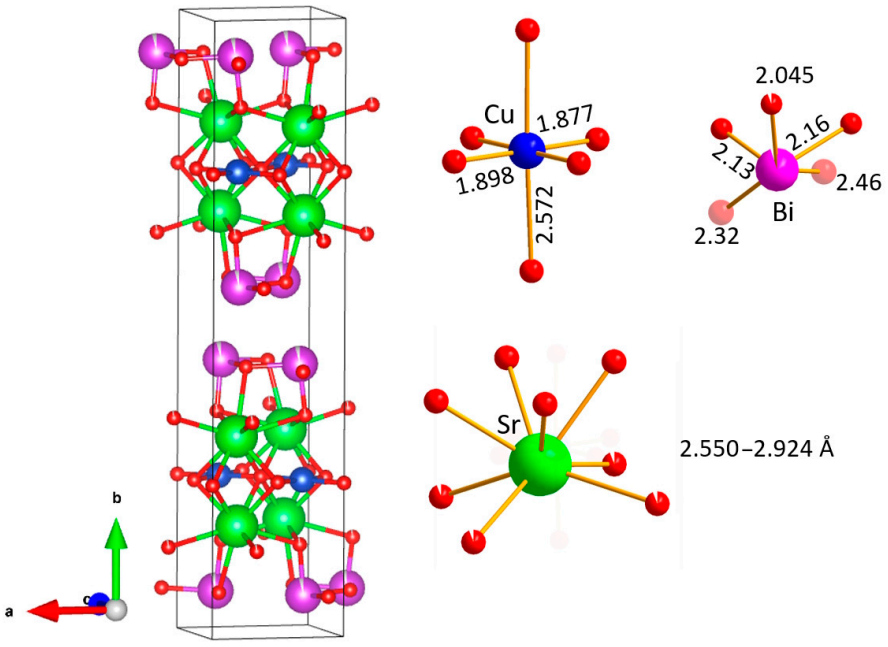

Figure 6. Crystal structure and coordination of heavy atoms in Pb-doped Bi-2201.

The crystal structure of a non-annealed OD3K crystal was also refined in the space group *Ccc*2 using 12,508 reflections measured ($3.318^\circ \leq 2\Theta \leq 61.82^\circ$), 1070 unique ($R_{int} = 0.1170$, $R_{sigma} = 0.0462$) in all calculations. The final R_1 was 0.0852 ($I > 2\sigma(I)$), and wR_2 was 0.1868 (all data). For comparison, refinement of the centrosymmetric space group *Cccm* converged to $R_1 = 0.1040$ ($I > 2\sigma(I)$) and $wR_2 = 0.2298$ (all data). The atomic coordinates, temperature factors, and site occupancies for the OD0K crystal, together with the details of the refinement, are listed in Tables S4–S6.

In Table 2, we put together different structural models proposed in the literature for the doped Bi-2201 and Bi-2212 compounds.

Table 2. A comparison of models reported for the average structure of superconducting doped Bi-2201 and Bi-2212.

	Present Study	**Ito et al. [34]**	**Imai et al. [51]**	**Gao et al. [40]**	**Gao et al. [36]**	**Tarascon et al. [52]**
Composition	$(Bi,Pb)_{1.902}Sr$ $CuO_{5.885}$	$Bi_{1.82}Pb_{0.32}Sr_{1.84}$ CuO_6	$Bi_2Sr_{1.60}Ca_{0.40}$ CuO_6	$Bi_{2.28}(Sr,Ca)_{1.72}$ CuO_6	$Bi_{2.14}Pb_{0.19}Sr_{1.11}Ca_{0.43}$ CuO_6	$Bi_{1.2}Pb_{0.8}Sr_{1.5}La_{0.5}$ CuO_6
Space group	*Ccc*2	*Cccm*	*Bbmb (Cccm)*	*A*2/*a*	*A*2*aa* (*Ccc*2)	*Pnan*
a, Å	5.3947(6)	5.392(3)	5.3826(8)	5.362(2)	5.3312(6)	5.328(1)
b, Å	24.605(3)	24.603(5)	5.376(1)	5.362(1)	5.3686(4)	5.415(1)
c, Å	5.2786(6)	5.300(3)	24.387(7)	24.30(1)	24.365(6)	24.383(1)
R	0.0478	0.048	0.109	0.104	0.105	0.10
R_w	0.112	0.077	0.108	0.111	0.117	0.14

Thus, the substitution of Bi by Pb yielded the observation of superconductivity in Bi-2201 materials that do not contain extra oxygen within the Bi-O layers. Also, this suggests a lowering of the oxygen content to 6 per formula unit. The subtle difference between structures with space groups *Ccc*2 and *Pnan* originates in the position of the oxygen atoms with respect to Bi in the Bi-O layers.

4. Summary and Conclusions

The crucible-free floating zone method has emerged as the most promising growth approach to obtain large-sized, compositionally homogeneous crystals of pure and Pb-doped Bi-2201. The FZ-grown Bi-2201 samples were always much larger and thicker along the *c*-axis compared with flux-prepared crystals and were suitable even for neutron scattering experiments. In contrast to pure Bi-2201, the Pb-doped samples grown by the FZ method reproducibly demonstrated superconducting properties after annealing in either a vacuum or in a reduced atmosphere.

Even highly Pb-overdoped Bi-2201 seemed to be prone to a weak modulation with $q \approx 0.21\ c^*$, which did not disappear even after post-annealing. We showed that these weak reflections can be convincingly described in the non-centrosymmetric space group *Ccc*2. The origin of non-centrosymmetricity is the position of the oxygen atoms with respect to Bi atoms in the Bi-O slabs. In Pb-doped Bi-2201 cuprates, there were no extra oxygens within the Bi-O layers, in contrast to undoped Bi-2201, e.g., Mironov et al. [30]. Superconductivity appeared in the non-annealed material at a critical temperature of 3 K and preserved in the annealed one with a T_c as high as 23 K.

Supplementary Materials: The following supporting information can be downloaded at: https://www.mdpi.com/article/10.3390/cryst14030270/s1. The atomic coordinates, temperature factors, and site occupancies for the Bi-2201 crystals, together with the details of the refinement, are listed in Tables S1–S6.

Author Contributions: All of the authors declare that they participated in the design, execution, and analysis of the paper: Crystal growth, A.M.; SCXRD investigation, M.R.; writing—original draft preparation, M.R. and A.M.; writing—review and editing, B.B.; project administration, A.M. and B.B. All authors have read and agreed to the published version of the manuscript.

Funding: The project received no external funding.

Data Availability Statement: The data presented in this study are available on request from the corresponding author.

Acknowledgments: The OD23K crystal was grown at the University of Amsterdam by Yingkai Huang and kindly provided for SCXRD measurements by Anna Isaeva and Mark Golden. Alexander Ovchinnikov and Laura Folkers are acknowledged for their help with the SCXRD data collection.

Conflicts of Interest: The authors declare no conflict of interest.

References

1. Zaanen, J.; Chakravarty, S.; Senthil, T.; Anderson, P.; Lee, P.; Schmalian, J.; Imada, M.; Pines, D.; Randeria, M.; Varma, C.; et al. Towards a Complete Theory of High Tc. *Nat. Phys.* **2006**, *2*, 138–143. [CrossRef]
2. Lee, P.A.; Nagaosa, N.; Wen, X.-G. Doping a Mott Insulator: Physics of High-Temperature Superconductivity. *Rev. Mod. Phys.* **2006**, *78*, 17–85. [CrossRef]
3. Keimer, B.; Kivelson, S.A.; Norman, M.R.; Uchida, S.; Zaanen, J. From Quantum Matter to High-Temperature Superconductivity in Copper Oxides. *Nature* **2015**, *518*, 179–186. [CrossRef]
4. Hashimoto, M.; Vishik, I.M.; He, R.-H.; Devereaux, T.P.; Shen, Z.-X. Energy Gaps in High-Transition-Temperature Cuprate Superconductors. *Nat. Phys.* **2014**, *10*, 483–495. [CrossRef]
5. Kurashima, K.; Adachi, T.; Suzuki, K.M.; Fukunaga, Y.; Kawamata, T.; Noji, T.; Miyasaka, H.; Watanabe, I.; Miyazaki, M.; Koda, A.; et al. Development of Ferromagnetic Fluctuations in Heavily Overdoped (Bi,Pb)$_2$Sr$_2$CuO$_{6+\delta}$ Copper Oxides. *Phys. Rev. Lett.* **2018**, *121*, 057002. [CrossRef]
6. Peng, Y.Y.; Fumagalli, R.; Ding, Y.; Minola, M.; Caprara, S.; Betto, D.; Bluschke, M.; De Luca, G.M.; Kummer, K.; Lefrançois, E.; et al. Re-Entrant Charge Order in Overdoped (Bi,Pb)$_{2.12}$Sr$_{1.88}$CuO$_{6+\delta}$ Outside the Pseudogap Regime. *Nat. Mater.* **2018**, *17*, 697–702. [CrossRef]
7. Wise, W.D.; Boyer, M.C.; Chatterjee, K.; Kondo, T.; Takeuchi, T.; Ikuta, H.; Wang, Y.; Hudson, E.W. Charge-Density-Wave Origin of Cuprate Checkerboard Visualized by Scanning Tunnelling Microscopy. *Nat. Phys.* **2008**, *4*, 696–699. [CrossRef]
8. Božović, I.; He, X.; Wu, J.; Bollinger, A.T. Dependence of the Critical Temperature in Overdoped Copper Oxides on Superfluid Density. *Nature* **2016**, *536*, 309–311. [CrossRef]
9. Piriou, A.; Jenkins, N.; Berthod, C.; Maggio-Aprile, I.; Fischer, Ø. First Direct Observation of the Van Hove Singularity in the Tunnelling Spectra of Cuprates. *Nat. Commun.* **2011**, *2*, 221. [CrossRef] [PubMed]
10. Ding, Y.; Zhao, L.; Yan, H.-T.; Gao, Q.; Liu, J.; Hu, C.; Huang, J.-W.; Li, C.; Xu, Y.; Cai, Y.-Q.; et al. Disappearance of Superconductivity and a Concomitant Lifshitz Transition in Heavily Overdoped $Bi_2Sr_2CuO_6$ Superconductor Revealed by Angle-Resolved Photoemission Spectroscopy. *Chin. Phys. Lett.* **2018**, *36*, 17402. [CrossRef]
11. Lim, S.; Varma, C.M.; Eisaki, H.; Kapitulnik, A. Observation of Broken Inversion and Chiral Symmetries in the Pseudogap Phase in Single- and Double-Layer Bismuth-Based Cuprates. *Phys. Rev. B* **2022**, *105*, 155103. [CrossRef]
12. Ivanov, A.A.; Ivanov, V.G.; Menushenkov, A.P.; Wilhelm, F.; Rogalev, A.; Puri, A.; Joseph, B.; Xu, W.; Marcelli, A.; Bianconi, A. Local Noncentrosymmetric Structure of $Bi_2Sr_2CaCu_2O_{8+y}$ by X-ray Magnetic Circular Dichroism at Cu K-Edge XANES. *J. Supercond. Nov. Magn.* **2018**, *31*, 663–670. [CrossRef]
13. Gotlieb, K.; Lin, C.-Y.; Serbyn, M.; Zhang, W.; Smallwood, C.L.; Jozwiak, C.; Eisaki, H.; Hussain, Z.; Vishwanath, A.; Lanzara, A. Revealing Hidden Spin-Momentum Locking in a High-Temperature Cuprate Superconductor. *Science* **2018**, *362*, 1271–1275. [CrossRef] [PubMed]
14. Chuang, Y.-D.; Gromko, A.D.; Fedorov, A.; Aiura, Y.; Oka, K.; Ando, Y.; Eisaki, H.; Uchida, S.I.; Dessau, D.S. Doubling of the Bands in Overdoped $Bi_2Sr_2CaCu_2O_8$: Evidence for *c*-Axis Bilayer Coupling. *Phys. Rev. Lett.* **2001**, *87*, 117002. [CrossRef] [PubMed]
15. Jacobs, T.; Katterwe, S.O.; Motzkau, H.; Rydh, A.; Maljuk, A.; Helm, T.; Putzke, C.; Kampert, E.; Kartsovnik, M.V.; Krasnov, V.M. Electron-Tunneling Measurements of Low-T_c Single-Layer $Bi_{2+x}Sr_{2-y}CuO_{6+\delta}$: Evidence for a Scaling Disparity between Superconducting and Pseudogap States. *Phys. Rev. B* **2012**, *86*, 214506. [CrossRef]
16. Katterwe, S.O.; Jacobs, T.; Maljuk, A.; Krasnov, V.M. Low Anisotropy of the Upper Critical Field in a Strongly Anisotropic Layered Cuprate $Bi_{2.15}Sr_{1.9}CuO_{6+\delta}$: Evidence for a Paramagnetically Limited Superconductivity. *Phys. Rev. B* **2014**, *89*, 214516. [CrossRef]
17. Chen, D.; Lin, C.; Maljuk, A.; Zhou, F. *Growth and Characterization of Bulk Superconductor Material*; Springer: Berlin/Heidelberg, Germany, 2016; ISBN 978-3-319-31548-5.
18. Chong, I.; Terashima, T.; Bando, Y.; Takano, M.; Matsuda, Y.; Nagaoka, T.; Kumagai, K. Growth of Heavily Pb-Substituted Bi-2201 Single Crystals by a Floating Zone Method. *Phys. C Supercond.* **1997**, *290*, 57–62. [CrossRef]
19. Remschnig, K.; Tarascon, J.M.; Ramesh, R.; Hull, G.W. Growth and Properties of Large Area $Bi_{2+x}Sr_{2-x}CuO_{6+y}$ Single Crystals. *Phys. C Supercond.* **1991**, *175*, 261–268. [CrossRef]

20. Gorina, J.I.; Kaljushnaia, G.A.; Martovitsky, V.P.; Rodin, V.V.; Sentjurina, N.N. Comparative Study of Bi2201 Single Crystalsgrown from Solution Melt and in Cavities Formed in KCl. *Solid State Commun.* **1998**, *108*, 275–278. [CrossRef]
21. Liang, B.; Maljuk, A.; Lin, C.T. Growth of Large Superconducting $Bi_{2+x}Sr_{2-y}CuO_{6+\delta}$ Single Crystals by Travelling Solvent Floating Zone Method. *Phys. C Supercond.* **2001**, *361*, 156–164. [CrossRef]
22. Sonder, E.; Chakoumakos, B.C.; Sales, B.C. Effects of Oxygen and Strontium Vacancies on the Superconductivity of Single Crystals of $Bi_2Sr_{2-x}CuO_y$. *Phys. Rev. B* **1989**, *40*, 6872–6877. [CrossRef]
23. Tanaka, I.; Kojima, H. Superconducting Single Crystals. *Nature* **1989**, *337*, 21–22. [CrossRef]
24. Takekawa, S.; Nozaki, H.; Umezono, A.; Kosuda, K.; Kobayashi, M. Single Crystal Growth of the Superconductor $Bi_{2.0}(Bi_{0.2}Sr_{1.8}Ca_{1.0})Cu_{2.0}O_8$. *J. Cryst. Growth* **1988**, *92*, 687–690. [CrossRef]
25. Matsumoto, M.; Shirafuji, J.; Kitahama, K.; Kawai, S.; Shigaki, I.; Kawate, Y. Preparation of $Bi_2Sr_2CuO_6$ Single Crystals by the Traveling Solvent Floating Zone Method. *Phys. C Supercond.* **1991**, *185–189*, 455–456. [CrossRef]
26. Oka, K.; Yamaguchi, H.; Ito, T. Crystal Growth of the Quasi-One-Dimensional Compound $Ca_{2+x}Y_{2-x}Cu_5O_{10}$. *Phys. B Condens. Matter* **2000**, *284–288*, 1390–1391. [CrossRef]
27. Wang, N.L.; Buschinger, B.; Geibel, C.; Steglich, F. Crystal Growth and Anisotropic Resistivity of $Bi_2Sr_{2-x}La_xCuO_y$. *Phys. Rev. B* **1996**, *54*, 7449–7454. [CrossRef] [PubMed]
28. Peng, J.B.; Lin, C.T. Growth and Accurate Characterization of $Bi_2Sr_{2-x}La_xCuO_{6+\delta}$ Single Crystals. *J. Supercond. Nov. Magn.* **2010**, *23*, 591–596. [CrossRef]
29. Torrance, J.B.; Tokura, Y.; LaPlaca, S.J.; Huang, T.C.; Savoy, R.J.; Nazzal, A.I. New Class of High Tc Structures: Intergrowth of Multiple Copper Oxide Perovskite-like Layers with Double Sheets of BiO. *Solid State Commun.* **1988**, *66*, 703–706. [CrossRef]
30. Mironov, A.V.; Petříček, V.; Khasanova, N.R.; Antipov, E.V. New Insight on Bismuth Cuprates with Incommensurate Modulated Structures. *Acta Cryst. B* **2016**, *72*, 395–403. [CrossRef] [PubMed]
31. Vojta, M. Lattice Symmetry Breaking in Cuprate Superconductors: Stripes, Nematics, and Superconductivity. *Adv. Phys.* **2009**, *58*, 699–820. [CrossRef]
32. Torardi, C.C.; Subramanian, M.A.; Calabrese, J.C.; Gopalakrishnan, J.; McCarron, E.M.; Morrissey, K.J.; Askew, T.R.; Flippen, R.B.; Chowdhry, U.; Sleight, A.W. Structures of the Superconducting Oxides $Tl_2Ba_2CuO_6$ and $Bi_2Sr_2CuO_6$. *Phys. Rev. B* **1988**, *38*, 225–231. [CrossRef]
33. Leligny, H.; Durčok, S.; Labbe, P.; Ledesert, M.; Raveau, B. X-ray Investigation of the Incommensurate Modulated Structure of $Bi_{2.08}Sr_{1.84}CuO_{6-\delta}$. *Acta Cryst. B* **1992**, *48*, 407–418. [CrossRef]
34. Ito, Y.; Vlaicu, A.-M.; Mukoyama, T.; Sato, S.; Yoshikado, S.; Julien, C.; Chong, I.; Ikeda, Y.; Takano, M.; Sherman, E.Y. Detailed Structure of a Pb-Doped $Bi_2Sr_2CuO_6$ Superconductor. *Phys. Rev. B* **1998**, *58*, 2851–2858. [CrossRef]
35. Tarascon, J.M.; LePage, Y.; McKinnon, W.R.; Ramesh, R.; Eibschutz, M.; Tselepis, E.; Wang, E.; Hull, G.W. New Non-Superconducting Modulation-Free $BiPbSr_2MO_y$ Phases (M = Co, Mn, Fe) Isotypic with the 10 K $Bi_2Sr_2CuO_y$ Superconductor. *Phys. C Supercond.* **1990**, *167*, 20–34. [CrossRef]
36. Gao, Y.; Lee, P.; Graafsma, H.; Yeh, J.; Bush, P.; Petricek, V.; Coppens, P. Incommensurate Modulations in the Lead-Doped Bismuth Strontium Calcium Copper Oxide 221 Superconducting Phase: A Five-Dimensional Superspace Description. *Chem. Mater.* **1990**, *2*, 323–328. [CrossRef]
37. Darriet, J.; Weill, F.; Darriet, B.; Zhang, X.F.; Etourneau, J. Crystal Structure of $Bi_2Sr_2CuO_6$: A Structure Based on Periodic Crystallographic Shear Planes in the "2201" Structure. *Solid State Commun.* **1993**, *86*, 227–230. [CrossRef]
38. Roth, R.S.; Rawn, C.J.; Bendersky, L.A. Crystal Chemistry of the Compound $Sr_2Bi_2CuO_6$. *J. Mater. Res.* **1990**, *5*, 46–52. [CrossRef]
39. Khasanova, N.R.; Antipov, E.V. Bi-2201 Phases Synthesis, Structures and Superconducting Properties. *Phys. C Supercond.* **1995**, *246*, 241–252. [CrossRef]
40. Gao, Y.; Lee, P.; Ye, J.; Bush, P.; Petricek, V.; Coppens, P. The Incommensurate Modulation in the $Bi_2Sr_{2-x}Ca_xCuO_6$ Superconductor, and Its Relation to the Modulation in $Bi_2Sr_{2-x}Ca_xCu_2O_8$. *Phys. C Supercond.* **1989**, *160*, 431–438. [CrossRef]
41. Walker, M.B.; Que, W. Structural Model for the Incommensurate Bismuth High-T_c Superconductors. *Phys. Rev. B* **1992**, *45*, 8085–8090. [CrossRef] [PubMed]
42. Yamamoto, A.; Takayama-Muromachi, E.; Izumi, F.; Ishigaki, T.; Asano, H. Rietveld Analysis of the Composite Crystal in Superconducting $Bi_{2+x}Sr_{2-x}CuO_{6+y}$. *Phys. C Supercond.* **1992**, *201*, 137–144. [CrossRef]
43. Zhao, L.; Zhang, W.-T.; Liu, H.-Y.; Meng, J.-Q.; Liu, G.-D.; Lu, W.; Dong, X.-L.; Zhou, X.-J. High-Quality Large-Sized Single Crystals of Pb-Doped $Bi_2Sr_2CuO_{6+\delta}$ High-Tc Superconductors Grown with Traveling Solvent Floating Zone Method. *Chin. Phys. Lett.* **2010**, *27*, 087401. [CrossRef]
44. Amano, T.; Tange, M.; Yokoshima, M.; Kizuka, T.; Nishizaki, S.; Yoshizaki, R. Co-Doping Effects of Pb and La in $(Bi,Pb)_2(Sr,La)_2CuO_y$. *Phys. C Supercond.* **2004**, *412–414*, 230–234. [CrossRef]
45. Ikeda, Y.; Hiroi, Z.; Ito, H.; Shimomura, S.; Takano, M.; Bando, Y. Bi, Pb-Sr-Cu-O System Including a Modulation-Free Superconductor. *Phys. C Supercond.* **1990**, *165*, 189–198. [CrossRef]
46. *APEX3, SAINT-Plus and SADABS*; Bruker AXS Inc.: Madison, WI, USA, 2016.
47. Krause, L.; Herbst-Irmer, R.; Sheldrick, G.M.; Stalke, D. Comparison of Silver and Molybdenum Microfocus X-ray Sources for Single-Crystal Structure Determination. *J. Appl. Cryst.* **2015**, *48*, 3–10. [CrossRef]
48. Sheldrick, G.M. SHELXT—Integrated Space-Group and Crystal-Structure Determination. *Acta Cryst. A* **2015**, *71*, 3–8. [CrossRef]
49. Sheldrick, G.M. A Short History of SHELX. *Acta Cryst. A* **2008**, *64*, 112–122. [CrossRef]

50. Gao, Y.; Lee, P.; Coppens, P.; Subramania, M.A.; Sleight, A.W. The Incommensurate Modulation of the 2212 Bi-Sr-Ca-Cu-O Superconductor. *Science* **1988**, *241*, 954–956. [CrossRef]
51. Imai, K.; Nakai, I.; Kawashima, T.; Sueno, S.; Ono, A. Single Crystal X-Ray Structure Analysis of $Bi_2(Sr, Ca)_2CuO_x$ and $Bi_2(Sr, Ca)_3Cu_2O_x$ Superconductors. *Jpn. J. Appl. Phys.* **1988**, *27*, L1661. [CrossRef]
52. Tarascon, J.M.; McKinnon, W.R.; LePage, Y.; Remschig, K.; Ramesh, R.; Jones, R.; Pleizier, G.; Hull, G.W. Superconductivity at 27 K in Modulation-Free $Bi_{2-x}Pb_xSr_{2-y}La_yCuO_6$ Phases with $X \cong y + 0.2$. *Phys. C Supercond.* **1990**, *172*, 13–22. [CrossRef]